Individual Differences in Women During Walking Affect Tibial Response to Load Carriage: The Importance of Individualized Musculoskeletal Finite-Element Models

Chun Xu, Jaques Reifman, Michael Baggaley, W. Brent Edwards, and Ginu Unnikrishnan

***Abstract*—Subject-specific features can contribute to the susceptibility of an individual to stress fracture. Here, we incorporated tibial morphology and material properties into a standard musculoskeletal finite-element (M/FE) model and investigated how load carriage influences joint kinetics and tibial mechanics in women. We obtained the morphology and material properties of the tibia from computed tomography images for women of three distinctly different heights, 1.51 m (short), 1.63 m (medium), and 1.75 m (tall), and developed individualized M/FE models for each. Then, we calculated joint and muscle forces, and subsequently, tibial stress/strain for each woman walking at 1.3 m/s under various load conditions (0, 11.3, or 22.7 kg). Among the subjects investigated, using individualized and standard M/FE models, the joint reaction forces (JRFs) differed by up to 4 (hip), 22 (knee), and 26% (ankle), and the 90th percentile von Mises stress by up to 30% (tall woman). Load carriage evoked distinct biomechanical responses, with a 22.7-kg load decreasing the peak hip JRF during late stance by ∼18% in the short woman, while increasing it by ∼39% in the other two women. It also increased peak knee and ankle JRFs by up to ∼48 (tall woman) and ∼36% (short woman). The same load increased the 90th percentile von Mises stress (and corresponding cumulative stress) by 31 (28), 22 (30), and 27% (32%) in the short, medium, and tall woman, respectively. Our findings highlight the critical role of individualized M/FE models to assess mechanical loading in different individuals performing the same physical activity.**

***Index Terms*—Stress fracture in women, tibial stress and strain, musculoskeletal finite-element analysis, load carriage.**

I. Introduction

STRESS fractures hinder military readiness, leading to substantial lost-duty days and increased medical costs [1]. This musculoskeletal injury, characterized by localized tissue damage and pain, is common among military recruits who abruptly engage in high-impact physical activities during basic combat training (BCT). The etiology of stress fracture is complex and multifactorial [2], and its contributing factors can be categorized into modifiable risk factors (e.g., external loading; training parameters including volume, pace, and intensity; training surface; and footwear [2]) or non-modifiable risk factors (e.g., bone mineral density (BMD), body size, skeletal alignment [2], sex, and race [3], [4]). Other physiological factors, such as bone turnover rate, flexibility, and muscular strength, as well as hormonal and nutritional factors, may also play a role in determining the risk of stress fracture [2]. In addition to understanding the contribution of individual risk factors, it is even more important to understand how the effects of each risk factor combine to generate composite estimates of risk, and to evaluate how these estimates relate to tissue mechanics.

A large body of evidence suggests that the development of stress fracture is analogous to that of fatigue failures in engineering material, in the sense that it is caused by a repetitive, fluctuating mechanical load [5]–[7], which during any one loading cycle, is substantially lower than the maximum load capacity of bones [8] and does not cause failure. For example, cyclic loads associated with weight-bearing physical activities during BCT may cause bones to undergo gradual mechanical failure, a process known as fatigue [9]. Over time, if the load is high enough to overwhelm the bone repair process that removes micro-cracks or reduces their size [10], bone fatigue may lead to macro-cracks or even biomechanical failure of the cortex (i.e., stress fracture) [11], [12]. The risk of stress fracture, in theory, is positively

Manuscript received September 27, 2018; revised February 7, 2019 and April 26, 2019; accepted May 9, 2019. Date of publication May 30, 2019; date of current version January 20, 2020. This work was supported in part by the U.S. Army Network Science Initiative and in part by a grant from the Defense Health Program managed by the Military Operational Medicine Program Area Directorate, U.S. Army Medical Research and Development Command, Fort Detrick, Maryland. *(Corresponding author: Jaques Reifman.)*

C. Xu and G. Unnikrishnan are with the Henry M. Jackson Foundation for the Advancement of Military Medicine, Inc. (HJF), and also with the Department of Defense, Biotechnology High Performance Computing Software Applications Institute (BHSAI), Telemedicine and Advanced Technology Research Center (TATRC), United States Army Medical Research and Development Command (USAMRDC).

J. Reifman is with the Department of Defense, Biotechnology High Performance Computing Software Applications Institute (BHSAI), Telemedicine and Advanced Technology Research Center (TATRC), United States Army Medical Research and Development Command (USAMRMC), Fort Detrick, MD 21702 USA (e-mail: jaques.reifman.civ@mail.mil).

M. Baggaley and W.B. Edwards are with the Human Performance Laboratory, Faculty of Kinesiology, University of Calgary, and also with the McCaig Institute for Bone and Joint Health, Cumming School of Medicine, University of Calgary.

Digital Object Identifier 10.1109/TBME.2019.2917415

related to the total number of loading cycles (i.e., the number of strides), as well as the magnitude of mechanical loading sustained by the bone within each cycle. Therefore, to reduce the risk of stress fracture, a necessary first step is to characterize the mechanical loading on the bone imposed by military-relevant physical activities.

To this end, we previously characterized the joint kinematics (joint angles), kinetics (joint reaction forces or JRFs), and tibial mechanics (stress and strain) of female subjects walking [5] and running [6] with and without load carriage, using standard musculoskeletal finite-element (M/FE) analyses. In the standard M/FE model, we estimated the bone dimensions and mass-inertia properties by linearly scaling a generic musculoskeletal model to match the height and weight of a specific subject. Then, we performed FE analyses using material properties derived from computed tomography (CT) images of a subject matched in terms of sex, age, and body mass index. This standard M/FE analysis provides task-specific characterization of joint kinematics, kinetics, and tibial mechanics when subjects perform the same physical activities under the same condition. However, it does not explain why only a small fraction of subjects undergoing the same amount of physical activity are more susceptible to stress fracture than others and how subject-specific features jointly contribute to an individual's injury susceptibility [13].

Risk factors contribute to the development of stress fracture in a specific individual, at least partially, by altering the mechanical loading on the bone, both independently and interactively [2]. Therefore, it is important to customize the standard M/FE analyses by considering key modifiable and non-modifiable risk factors that may predispose a specific individual to stress fracture during BCT. Here, we sought to extend our previous work and answer the following research question: how does incorporation of subject-specific tibial features, such as shape and size, in a standard M/FE model affect model predictions? To answer this question, as an example, we investigated the changes in the joint kinetics and tibial response of women of different body sizes when walking while carrying a load. We tested the hypothesis that an individualized M/FE model makes it possible to distinguish biomechanical responses among anthropometrically different women during walking.

II. Methods

We modified a previously reported method [5], [6] to develop individualized M/FE analyses by incorporating subject-specific features of the tibiae into standard M/FE analyses. We chose the tibia as the bone of interest because it is the most frequent site of stress fracture in athletes [14] and military recruits [15]. We chose female subjects because of the growing number of women serving in the Army and their higher risk for developing stress-fracture injuries than men [16].

A. Participant Characteristics

To ensure that study subjects were representative of Army recruits [17], we enrolled three healthy, young, adult women without any self-reported history of bone disorders or lower limb stress fractures. We enrolled one "short" woman [height, 1.51 m; mass, 55.2 kg; body mass index (BMI), 24.2 kg/m^2; fat percentage, 21.1%; age, 19 yr], one "medium" woman (height, 1.63 m; mass, 64.0 kg; BMI, 24.1 kg/m^2; fat percentage, 26.4%; age, 20 yr), and one "tall" woman (height, 1.75 m; mass, 71.8 kg; BMI, 23.4 kg/m^2; fat percentage, 15.9%; age, 20 yr) for this study. We received approval from the Human Research Protection Office at the U.S. Army Medical Research and Development Command (Ft. Detrick, MD) and the Conjoint Health Research Ethics Board of the University of Calgary (Calgary, AB, Canada). We obtained informed written consent from each participant prior to the study.

B. Collection of Imaging and Motion-Capture Data

For each subject, we obtained CT scans of the left leg, using a GE Discovery Scanner (General Electric Medical System, Milwaukee, WI) with acquisition settings of 120 kVp and 200 mAs. Images were reconstructed with a slice thickness of 0.63 mm and an in-plane pixel resolution of 0.49 mm $\times$ 0.49 mm. Each CT scan included a calibration phantom with known calcium hydroxyapatite concentrations (QRM, Moehrendorf, Germany), which allowed us to determine the apparent bone density from the Hounsfield units (HU) in the CT dataset.

We collected motion-capture data for subjects walking on an instrumented treadmill (Bertec, Columbus, OH), including walking at 1.3 m/s carrying no load (0 kg, baseline model) or a load of 11.3 or 22.7 kg (i.e., 25 or 50 lb) using a weight vest. The 11.3 or 22.7 kg was equivalent to 20.5, 17.7, and 15.8% of the body weight (BW) or 41.1, 35.4, and 31.6% BW for the short, medium, and tall woman, respectively. Before each motion-capture experiment, we secured 42 retroreflective markers on anatomical landmarks and segments of the subject's body, and used an eight-camera motion analysis system (Vicon Nexus, Centennial, CO) to track their positions. Then, we conducted static trials to establish segmental coordinate systems. We collected motion and force-platform data at sampling frequencies of 200 and 1000 Hz, respectively. For each experimental condition, we collected data for a minimum of 15 strides after subjects were observed to have reached a consistent gait pattern. We randomized the order of walking tasks, and encouraged subjects to take adequate rest and hydrate between each condition, as necessary. For each subject under each load-carriage condition, we determined the preferred stride length for at least nine consecutive strides, and averaged them to obtain a representative value.

C. Standard Musculoskeletal Analysis

We first performed a standard musculoskeletal analysis by scaling a generic female musculoskeletal model based on the Twente Lower Extremity Model 2.0 [18], which is available in the AnyBody Modeling System (AnyBody Technology, Aalborg, Denmark) [5], [6]. This generic model, originally constructed from medical imaging data and cadaver dissection, included musculoskeletal geometries, muscle wrapping surfaces, muscle-tendon attachment sites, and lines of action [19].

Then, we used anthropometric measurements (i.e., height, mass, and fat percentage) to scale bone dimensions and mass-inertia properties in the generic model for our three women. As in our previous work [5], [6], we modeled the hip joints as spherical joints, and the knee and ankle joints as revolute joints. We simplified the knee joint as a revolute joint connecting the patella to the femur, which allowed a small degree of rotation but no translation.

D. Incorporation of Subject-Specific Tibiae

To develop a musculoskeletal model with subject-specific tibiae (i.e., the individualized model), we morphed the generic tibia into the geometry of the subject-specific tibia through a sequence of affine (linear) and non-affine transformations using a method similar to that reported by Marra *et al.* [20]. This procedure is required to accurately represent the different muscle-attachment locations in each individualized model. We morphed the generic tibia in three steps, as detailed below.

First, we obtained the surface mesh of the generic tibia (termed the *source* mesh) by extracting the outer surface of the left tibia from the standard model. This *source* tibia was defined in an anatomical reference coordinate system within the standard model, whose y-direction was aligned with the long axis of the tibia. Next, we obtained the geometry of the subject-specific tibia from the CT images, with the long axis of the tibia aligned with the z-direction of the CT image coordinate system. Finally, we created the surface mesh of the subject-specific tibia (termed the *target* mesh) using a host-mesh fitting method [21], wherein the *source* mesh was deformed into the geometry of the subject-specific tibia. This approach ensured topological equivalence between the *source* and *target* meshes so that they had the same number of elements and vertices, and that each corresponding element represented the same anatomical features.

Second, we scaled and registered the *source* and *target* tibial meshes using linear affine transformations, which included translation, rotation, scaling, and skewing of the meshes. Next, we performed a tri-harmonic radial basis function interpolation to account for the local anatomical details in the meshes, which were not captured by the linear transformations. This procedure produced a morphed *source* tibia whose geometry and location coincided with those of the *target* tibia, which was defined within the CT image coordinate system. Importantly, all associated soft tissue attachment points were deformed together with the tibial geometry.

Lastly, we used a reverse rigid-body transformation to translate the morphed *source* mesh from the CT image coordinate system to the anatomical reference coordinate system within the musculoskeletal model.

Subject-specific morphing was not possible for the remaining bones of the musculoskeletal model because CT scans were lacking. Therefore, the remaining bone segments were defined using anthropometric scaling and an optimization scheme described by Andersen *et al*. [22]. This method determines the joint centers and axes through a least-squares parameter identification algorithm that minimizes the errors between markers defined in the model and those tracked in the experiment. Assuming symmetry between the left and right legs, we constructed a mirror transformation function to morph the right tibia. To quantify the discrepancy in tibial geometry estimation, we compared the lengths of the subject-specific tibia reconstructed from CT images (i.e., used in the individualized musculoskeletal analysis) and the anthropometrically scaled tibia (i.e., used in the standard musculoskeletal analysis).

E. Inverse Dynamics

We adopted a functional-depth method [23] to identify the most representative stride from among the multiple strides acquired by the motion-capture experiments, in order to drive the standard (i.e., the anthropometrically scaled model) and individualized (i.e., the anthropometrically scaled model with subject-specific tibiae) musculoskeletal analyses. For the standard and individualized models, we used an inverse dynamics approach to compute muscle activities and then joint reaction forces (JRFs) during walking. We defined the muscle activity as the muscle force divided by muscle strength [24]. In our models, JRF refers to a resultant quantity that includes forces across the articulating surfaces and forces from muscular contraction. We performed whole-body musculoskeletal analyses for walking without load, or with an 11.3- or 22.7-kg load for all subjects. We quantified the role of subject-specific tibiae in musculoskeletal analysis by comparing the JRFs predicted by the standard and individualized analyses. We used the Kolmogorov-Smirnov two-sample test to test for equivalence of JRFs between the two models.

F. Finite Element Analysis

We used a method similar to our previous work [5], [6] to perform the FE analysis. Briefly, we created a 10-node quadratic tetrahedral mesh (C3D10) with an average edge-length of 3.5 mm (determined using a mesh convergence study) from the surface mesh of the *target* geometry. Then, we converted the HU values obtained from the CT images into apparent densities, and then to elastic moduli based on the calibration phantom [25], [26] for each voxel of the CT images. Subsequently, we mapped the voxel-based properties to the elements of the subject-specific tibial FE mesh [27], and grouped them into discrete material property bins with a gap of 50 MPa between two adjacent bins. This procedure produced approximately 200,000 unique material property definitions for the tibia model. We represented the bone and intramedullary tissue regions as linear elastic and isotropic materials. We assigned Poisson's ratios of 0.325 and 0.167 for the bone region (HU $>$ 100) and intramedullary tissue region (HU $<$ 100), respectively [28].

We used the muscle forces and joint forces/moments obtained from the musculoskeletal analysis as the loading conditions for the FE analysis. Specifically, we defined the muscle/ligament insertion points in the musculoskeletal model as FE constraint nodes, which in turn were coupled to the outer surface of the tibial FE meshes. Through this procedure, on average, we specified 171 couplings between the muscle/ligament nodes and the

tibial FE meshes. We defined the bone-to-bone contact forces in a similar manner.

Using an in-house-developed Tool Command Language script, we generated an ABAQUS input file for structural analysis to determine the spatiotemporal tibial stress distribution during one gait cycle (ABAQUS Explicit 6.12, Dassault Systèmes, Vélizy-Villacoublay, France). We obtained the cumulative tibial stress during a stride by integrating the predicted nodal stress values over time for all nodes in the tibial FE model [5], [6].

We created FE models from the standard musculoskeletal model for each of the three individuals. Then, we compared the tibial stresses predicted by the individualized and standard FE models for walking without a load. For constructing the standard models, we used subject-specific tibial material properties, using a mesh-morphing and material-property mapping algorithm [5], with the loading derived from the standard musculoskeletal models from each of the three subjects. In this way, we were able to assess the effect of standard geometry and loading on FE-predicted tibial stress.

III. Results

A. Importance of Subject-Specific Tibial Features

We observed considerable differences in size and shape between the anthropometrically scaled (Fig. 1(a), blue) and subject-specific tibiae (Fig. 1(a), yellow). For example, the anthropometrically scaled tibia overestimated the tibial length in all subjects (by 29, 10, and 2 mm for the short, medium, and tall woman, respectively).

These morphological differences led to quantitative differences in the predicted JRFs between the standard and the individualized musculoskeletal models by up to 3.6, 21.7, and 25.8% at the hip, knee, and ankle, respectively (Table I). Specifically, for the short woman walking with a load of 22.7 kg (50 lb), the differences in the peak values of the knee and ankle JRFs ranged from 6.9 to 24.9% (Fig. 1(b) and Table I). Kolmogorov-Smirnov tests to compare peak JRFs at the hip, knee, and ankle between the standard and individualized models revealed statistically significant differences in knee JRFs in the anterior-posterior direction, as well as ankle JRFs in the medial-lateral and proximal-distal directions ($p < 0.05$, Table I).

Moreover, the material properties of the tibia, estimated from the subject-specific CT images, showed similar patterns among all subjects, with Young's modulus in the middle third of the diaphysis being higher than that in the remaining regions of the tibia (Fig. 2). Overall, Young's modulus was higher for the tall woman (peak, 22.1 GPa) than for the short (peak, 19.0 GPa) or medium (peak, 18.9 GPa) woman.

Owing to the differences in the tibial morphology (Fig. 1(a)) and the internal forces during a stride (Fig. 1(b)), when compared to the individualized FE models, the standard FE models overestimated the 90th percentile von Mises stress by 13.0% (29.3 vs. 33.1 MPa) for the short woman, and underestimated it by 18.9% (42.3 vs. 34.3 MPa) for the medium women and by 30.1% (52.1 vs. 36.4 MPa) for the tall woman (Fig. 3).

B. Joint Kinetics in Response to Load Carriage

The JRF profiles largely reflected the shapes of the ground reaction forces (GRFs) (Fig. 4). In all subjects under all load conditions, we observed two well-defined peaks, GRF_1 and GRF_2, which occurred during the early (i.e., ∼25%) and late (i.e., ∼50%) phases of the stance, respectively. The GRF measurements for the tall woman were greater than those for the other two women (Fig. 4 and Table II). In contrast to the medium woman and tall woman, who demonstrated similar magnitude for both GRF_1 and GRF_2 measurements, the short woman illustrated GRF_1 measurements that were greater than GRF_2 measurements by 16.7, 14.3, and 25.0% when she walked with loads of 0, 11.3, and 22.7 kg, respectively (Table II). As a result of this unique GRF profile, with an additional load of 22.7 kg (41.1% BW), her peak hip JRF increased by 56.7% during early stance but decreased by 18.2% during late stance. In contrast, in the medium woman and tall woman, the hip JRFs increased by ∼27.0% during early stance and by ∼39.0% during late stance.

In the tall woman, an extra load of 11.3 or 22.7 kg increased her peak knee JRF by 20.0 or 48.0%, respectively, for the two loads (Table II). Moreover, under all loading conditions, the tall woman demonstrated the highest peak knee JRFs (Fig. 4 and Table II). Lastly, load carriage increased ankle JRFs in all subjects. The peak ankle JRF in the short woman was more sensitive to load carriage, as evidenced by an increase of 14.3 or 35.7% in response to a load of 11.3 or 22.7 kg, respectively (Fig. 4 and Table II).

C. Tibial Stress, Cumulative Stress, and Strain in Response to Load Carriage

For all subjects under all load conditions, high stresses were concentrated in the middle third of the diaphysis, with the magnitude of compressive stress in the posterior aspect being greater than that of tensile stress in the anterior crest of the tibia (Fig. 5).

Compared to the baseline condition, an additional 22.7 kg increased the 90th percentile von Mises stresses from 29.3 to 38.4 MPa (a 31.1% increase) in the short woman; from 42.3 to 51.7 MPa (a 22.2% increase) in the medium woman; and from 52.1 to 66.1 MPa (a 26.9% increase) in the tall woman. Moreover, when the tall woman carried a load of 22.7 kg, the 90th percentile von Mises stress (i.e., 66.1 MPa) was 72.1% greater than that in the short woman (i.e., 38.4 MPa) and 27.9% greater than that in the medium woman (i.e., 51.7 MPa) (Table III).

The cumulative stress, which we obtained by integrating the von Mises stress across the loading time (i.e., one cycle) increased with an increase in the load carriage. For example, the 90th percentile cumulative stress in the short woman, when compared to the no-load condition, increased by 27% when carrying a load of 22.7 kg (Table III). The same load increased the 90th percentile cumulative stress in the medium woman and tall woman by 30 and 32%, respectively. While the 90th peak cumulative stress for the short woman was 36.6% lower than of the tall women with a load of 22.7 kg, for the medium woman the peak cumulative stress was only 1.7% lower than that of the tall women (Table III).

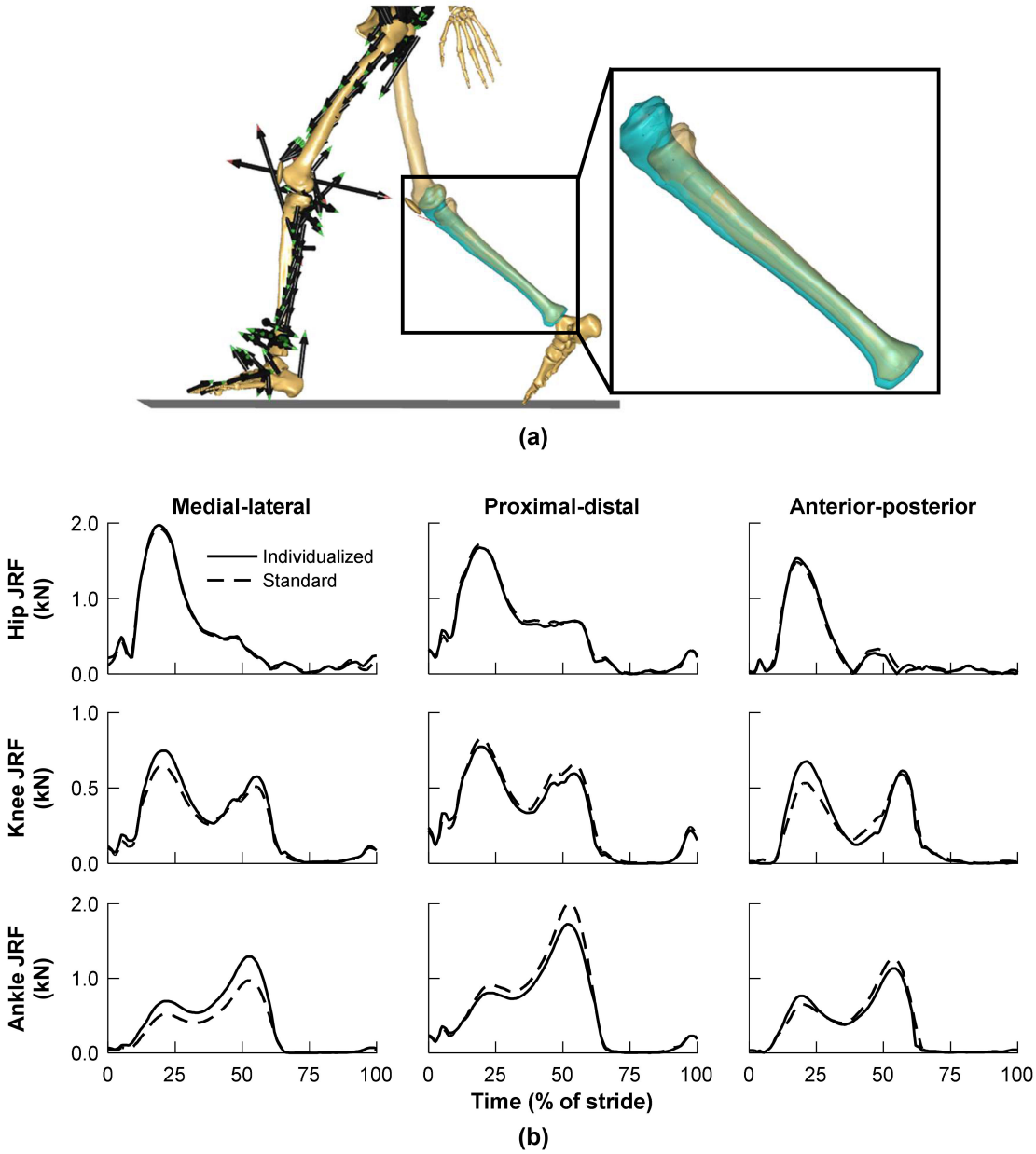

Fig. 1. (a) Subject-specific tibial data were incorporated into the musculoskeletal model to simulate the short woman walking with a load of 22.7 kg (50 lb). The musculoskeletal forces (arrows) predicted by the individualized model (yellow) are depicted on the left leg. The scaled generic tibia used in the standard model (blue) was superimposed on the right leg to show morphological differences. (b) Differences between the joint reaction forces (JRF) predicted by the individualized and standard models were more pronounced in the anterior–posterior direction at the knee, as well as in the medial-lateral and proximal-distal directions at the ankle. The proximal-distal direction is aligned with the long axis of the tibia.

Lastly, similar to the increase in von Mises and cumulative stresses, a load of 22.7 kg increased the 90th percentile maximum compressive strain from 1906.8 to 2485.8 $\mu\varepsilon$ (a 30.4% increase) in the short woman; from 2708.0 to 3310.4 $\mu\varepsilon$ (a 22.2% increase) in the medium woman; and from 2839.4 to 3491.5 $\mu\varepsilon$ (a 23.0% increase) in the tall woman (Table III).

IV. Discussion

In the present work, we investigated the influence of subject-specific features on the joint kinetics and tibial mechanics in three women of distinct body sizes walking at 1.3 m/s, using individualized M/FE analyses.

In support of our hypothesis, the joint kinetics and tibial stress distributions predicted by the standard and individualized M/FE models differed substantially. These results suggest that subject-specific bone morphology, such as size and shape, may be critical in estimating body kinetics and should therefore be incorporated into musculoskeletal models. For example, the standard musculoskeletal model overestimated the tibial length by as much as 29 mm in the short woman (Fig. 1(a)). This discrepancy leads to less accurate estimation of muscle moment

TABLE I
INDIVIDUALIZED VERSUS STANDARD MODELS

	Short			Medium			Tall		
Load carriage (kg)									
	0.0	11.3	22.7	0.0	11.3	22.7	0.0	11.3	22.7
Hip JRF (%)									
Medial-lateral	3.1	1.9	2.1	0.4	0.3	0.4	0.2	1.4	1.4
Proximal-distal	1.8	0.4	2.5	0.9	3.1	2.2	1.4	1.3	2.5
Anterior-posterior	1.4	2.2	3.6	1.2	1.7	1.2	3.3	2.0	1.8
Knee JRF (%)									
Proximal-distal	7.2	5.9	6.9	0.3	1.8	0.3	1.2	1.1	2.0
Anterior-posterior	19.4*	21.7*	12.7*	13.5	19.9*	17.8*	3.3	11.2	11.9
Ankle JRF (%)									
Medial-lateral	25.5*	25.8*	24.9*	18.8*	19.3*	20.0*	16.2*	18.3*	18.1*
Proximal-distal	11.9	14.5*	15.9*	3.6	3.0	2.7	1.2	1.4	1.0
Anterior-posterior	8.0	10.0	11.3	0.8	0.1	0.4	2.2	2.0	0.2

Differences in predicted joint reaction force (JRF) components in the medial-lateral, proximal-distal, and anterior-posterior directions between the individualized and standard models at the hip, knee, and ankle when subjects walked without a load (0.0 kg), or with an additional load of 11.3 or 22.7 kg, for the short woman, medium woman, and tall woman.

*$p < 0.05$: indicates a statistically significant difference between the JRFs predicted by individualized and standard models.

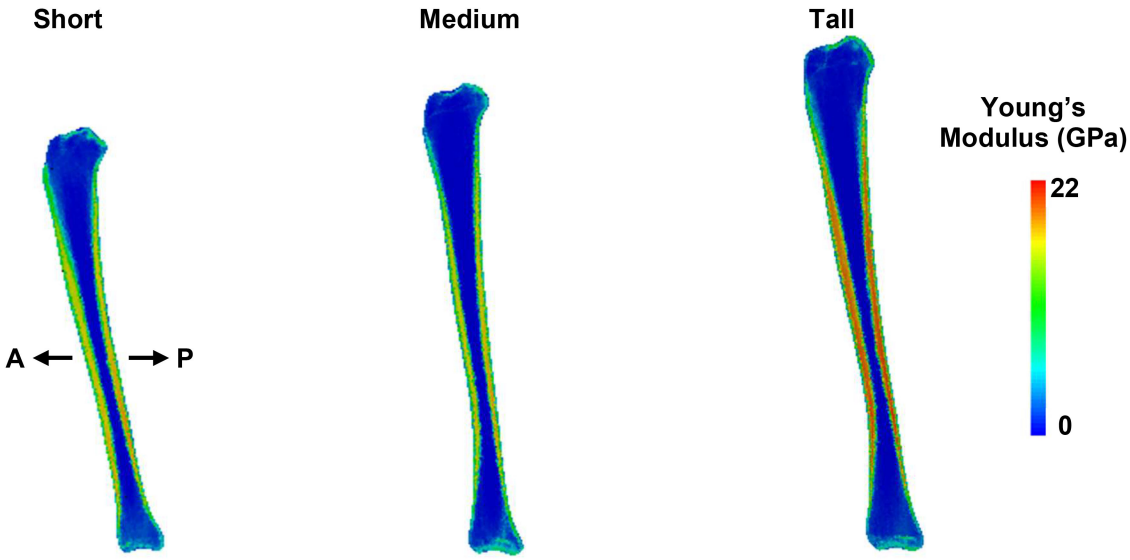

Fig. 2. Tibial geometries and material properties acquired from CT images for the short woman, medium woman, and tall woman. The material properties are superimposed on sagittal cross sections, which are arranged with the anterior (A)–posterior (P) axis running parallel to the page.

arms (which depends on the identification of muscle-tendon lines of action [29]), and inaccurate estimation of joint kinetics (e.g., more than a 25.0% discrepancy in ankle JRFs in the short woman, Table I). Ultimately, the discrepancies in subject-specific features, such as tibial morphology and JRFs, led to substantial differences in the predicted tibial stress distributions between the individualized and standard FE models (e.g., more than a 30% discrepancy in the 90th percentile tibial von Mises stress in the tall woman, Fig. 3).

Using the individualized M/FE model, we observed significant differences in the joint kinetics and tibial mechanics of these women during walking with load carriage. At baseline, the magnitude of tibial mechanical loading in the tall woman was greater than that in the short and medium woman (Table II). As expected, load carriage increased peak JRFs at the knee and the ankle in all three women. At the hip, a load of 22.7 kg increased peak hip JRFs in the medium and tall woman by ∼27.0% during early stance and by ∼39.0% during late stance. In contrast, in

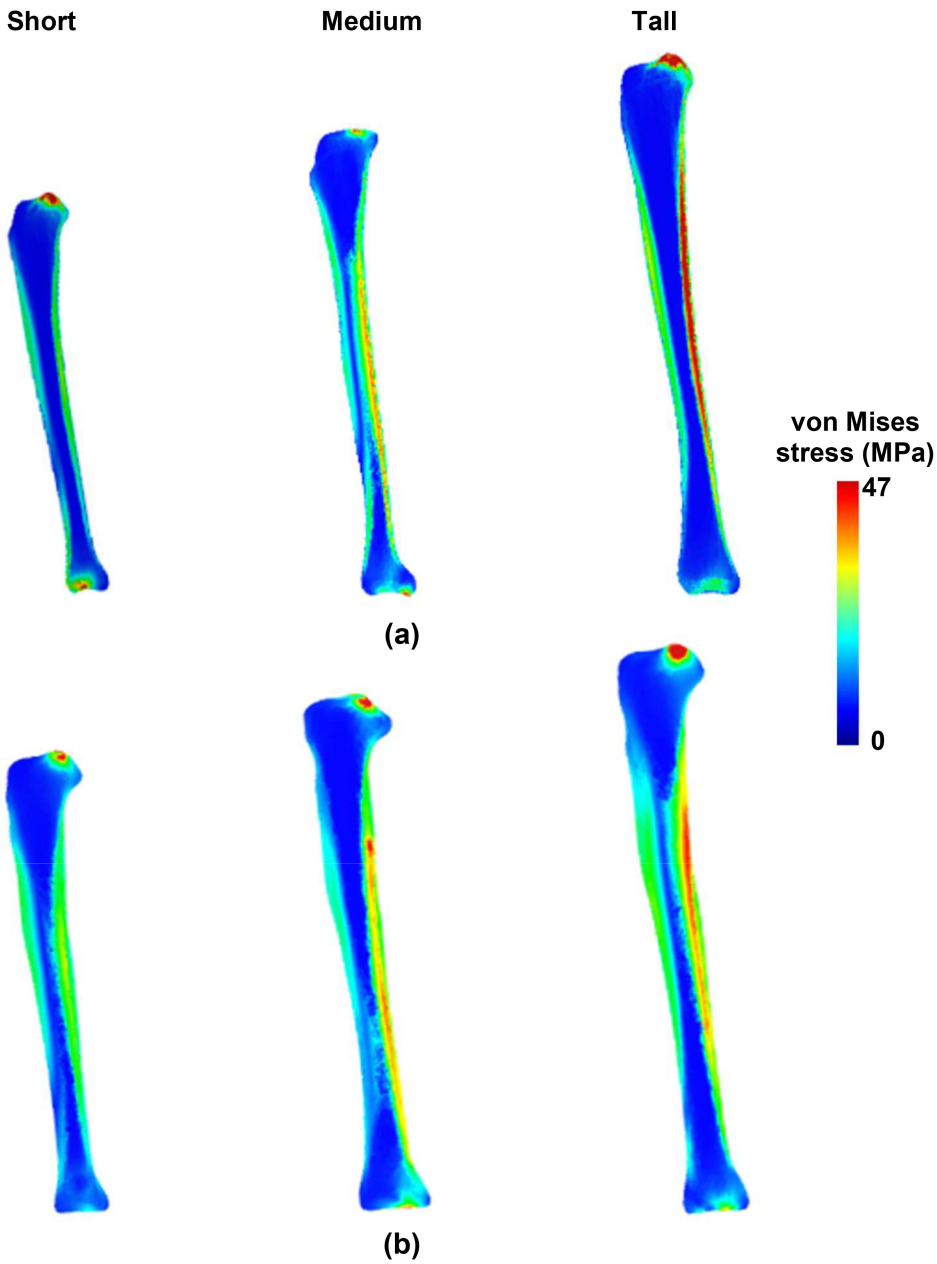

Fig. 3. Peak tibial stress distribution in the left leg for the short woman, medium woman, and tall woman walking without an additional load, predicted by the (a) individualized and (b) standard M/FE models. The images show cross-sections in the sagittal plane.

the short woman, a load of 22.7 kg (i.e., 41.1% BW) increased her peak hip JRF by 56.7% during early stance but decreased it by 18.2% during late stance (Table II).

The tibial von Mises stress and cumulative stress were different between the three subjects. In the posterior aspect of the middle third of the diaphysis, a load of 22.7 kg increased the 90th percentile maximum compressive stress by 31.1, 22.2, and 26.9% and the 90th percentile maximum compressive strain by 30.4, 22.2, and 23.0% in the short, medium, and tall woman, respectively. After integrating across loading time, the 90th percentile cumulative stress within one stride increased by 27.5, 30.4, and 31.7% in the short, medium, and tall woman, respectively (Table III). Overall, when incorporating subject-specific bone morphology and material properties (i.e., BMD) from CT images with physiologically accurate loading conditions from musculoskeletal analysis, individualized FE models produce arguably more realistic stress and strain distributions in the tibia than those produced by standard M/FE models [30]. The above results highlight the importance of individualized modeling approach in determining the FE-predicted tibial stress.

An individualized musculoskeletal model can provide complementary insight into the interaction of different factors influencing the mechanical load and, ultimately, the risk of stress fracture in the tibia. For example, at baseline, the short woman had lower internal forces than the medium woman and tall woman (Table II), which may be influenced by their difference

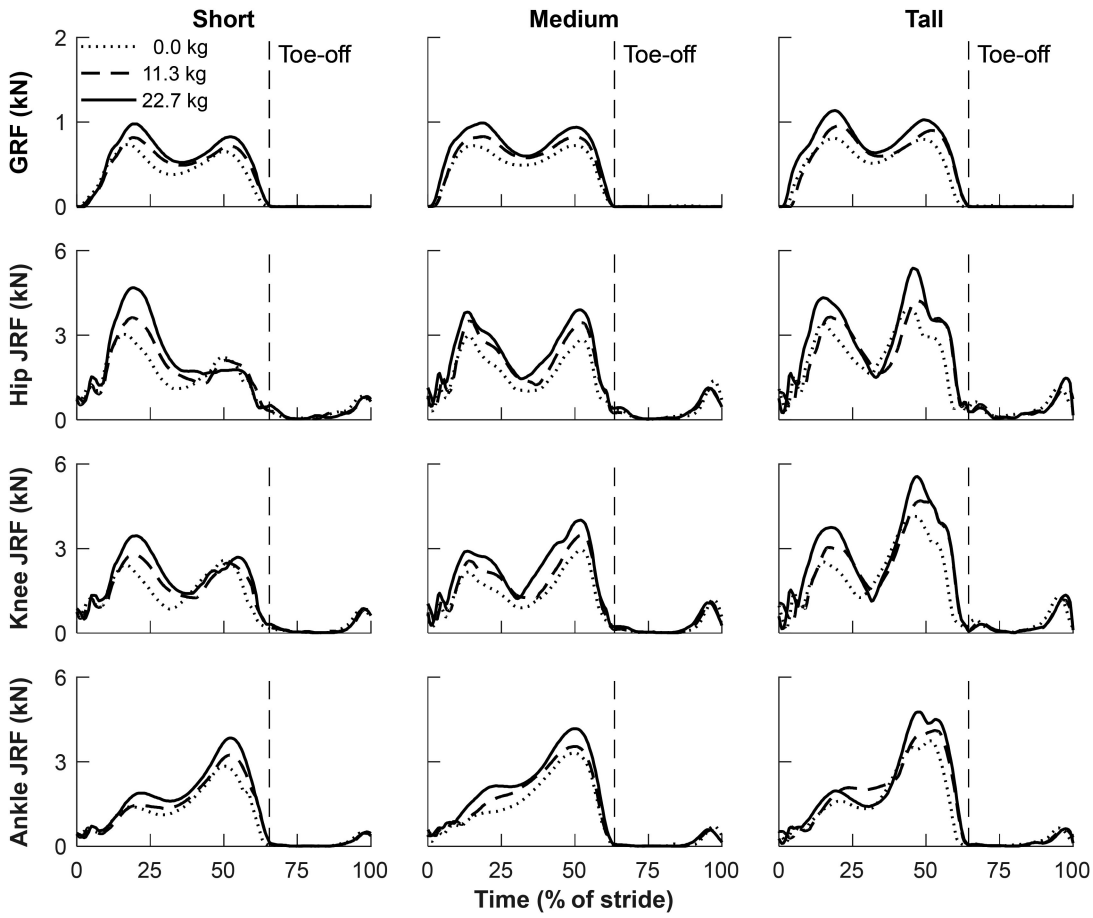

Fig. 4. Resultant joint reaction forces (JRF) at the hip, knee, and ankle under different loads during one gait cycle. Each graph begins and ends at initial contact. The vertical dashed line, which represents the toe-off point, separates the stance phase (before toe-off) from the swing phase (after toe-off). For convenience, the first row shows ground reaction forces (GRF).

in mass [i.e., the mass of the short woman (55.2 kg) was 15.9% lower than that of the medium woman (64.0 kg) and 30.1% lower than that of the tall woman (71.8 kg)]. Moreover, the stress, strain, and cumulative stress were smaller in the short woman than in the other women considered in this study (Table III). However, an applied load of 22.7 kg markedly changed the internal forces in the short woman relative to those in the medium woman and tall woman. Under this load condition, the hip JRF during the early stance phase of the short woman (4.7 kN) was 23.7% greater than that of the medium woman (3.8 kN) and 9.3% greater than that of the tall woman (4.3 kN) (Table II). These results show that, to identify whether an individual is predisposed to stress fracture, risk factors, such as body size, motion characteristics, and bone morphology, should be analyzed concurrently, which require individualized M/FE models.

Similar to previous studies [5], in all three women, the peak tibial strain during one stride (3491.5 $\mu\varepsilon$, tall woman) was below the experimentally determined threshold for the onset of microdamage (4000 $\mu\varepsilon$) [31], even when carrying a load as heavy as 22.7 kg (Table III). However, in addition to the magnitude of strain within one stride, the cumulative effect of mechanical loading, which is dependent on the duration of the stance phase (i.e., the duration of foot-ground contact time) and the total number of loading cycles (distance divided by stride length), plays an important role in how the bone responds to mechanical loading [32]. Our results suggest that when walking with a load of 22.7 kg, the 90th percentile von Mises stress in the tall woman (i.e., 66.1 MPa) was 27.9% greater than that in the medium woman (i.e., 51.7 MPa) and 72.1% greater than that in the short woman (i.e., 38.4 MPa, Table III). However, after integrating across loading time within one stride, the 90th percentile cumulative stress in the tall woman (i.e., 18.3 MPa·s) was only 1.7% greater than that in the medium woman (i.e., 18.0 MPa·s) and 57.8% greater than that in the short woman (i.e., 11.6 MPa·s, Table III).

Assuming no fatigue and a constant stride length during a one-mile ruck march with a load of 22.7 kg, the cumulative tibial stress [cumulative stress per walking cycle (Table III) $\times$ number of steps to cover a mile] would reach 21.4, 21.5, and 14.5 GPa·s in the tall, medium, and short woman, respectively. In other words, the differences in biomechanical impact on the tibia as a result of marching for one mile with a load of 22.7 kg are essentially negligible between the tall women and the medium woman (-0.2%), but still substantial between these women and the short woman ($\sim$48%). If the cumulative effect of internal

TABLE II
JOINT KINEMATICS AND KINETICS

	Short			Medium			Tall		
Load carriage (kg)									
	0.0	11.3	22.7	0.0	11.3	22.7	0.0	11.3	22.7
Stride length (mm)									
	1297.8	1303.6	1288.4	1380.2	1365.7	1350.6	1384.5	1365.7	1375.8
Ground reaction force (kN)									
Early stance	0.7	0.8	1.0	0.7	0.8	1.0	0.8	1.0	1.1
Late stance	0.6	0.7	0.8	0.7	0.8	0.9	0.8	0.9	1.0
Peak joint moment (N·m)									
Hip									
Flexion	35.9	31.3	18.6	58.8	72.0	79.5	56.8	72.0	76.5
Extension	62.7	65.4	91.5	44.7	48.8	59.9	54.8	58.8	62.5
Knee									
Flexion	25.9	23.5	27.2	19.0	25.1	38.4	62.4	71.0	82.5
Extension	26.0	33.2	31.9	32.4	40	48.4	22.6	39.0	59.5
Ankle									
Plantarflexion	86	95.7	110.1	100.2	110.8	130.9	120.1	139.7	140.8
Peak joint reaction force (kN)									
Hip									
Early stance	3.0	3.6	4.7	3.0	3.5	3.8	3.4	3.6	4.3
Late stance	2.2	2.1	1.8	2.8	3.5	3.9	3.9	4.2	5.4
Knee									
Early stance	2.4	2.8	3.4	2.2	2.6	2.9	2.5	3.0	3.7
Late stance	2.6	2.5	2.7	2.9	3.5	4.0	4.1	4.7	5.6
Ankle	2.8	3.2	3.8	3.3	3.5	4.2	3.7	4.1	4.8

Peak joint moments and joint reaction forces at the hip, knee, and ankle when subjects walked without a load (0.0 kg), or with an additional load of 11.3 kg (25 lb) or 22.7 kg (50 lb), for the short woman, medium woman, and tall woman.

TABLE III
MODEL PREDICTED VON MISES STRESS, CUMULATIVE STRESS, AND STRAIN

Load carriage (kg)	Short			Medium			Tall		
	10^{th}	50^{th}	90^{th}	10^{th}	50^{th}	90^{th}	10^{th}	50^{th}	90^{th}
von Mises Stress (MPa)									
0.0	9.7	22.8	29.3	12.3	27.2	42.3	14.5	36.6	52.1
11.3	11.1	24.0	30.4	12.5	30.8	47.3	16.1	41.1	58.5
22.7	12.5	28.9	38.4	14.2	33.7	51.7	18.2	46.9	66.1
Cumulative Stress (MPa·s)									
0.0	3.6	6.7	9.1	4.6	9.9	13.8	5.3	11.0	13.9
11.3	3.9	7.8	10.7	5.2	11.5	16.3	6.1	13.4	17.4
22.7	4.4	8.6	11.6	5.8	13.0	18.0	6.6	14.4	18.3
Maximum Compressive Strain (με)									
0.0	860.8	1516.3	1906.8	1041.6	1990.4	2708.0	1032.5	2090.4	2839.4
11.3	967.8	1588.3	1969.0	1128.1	2169.2	2939.0	1169.3	2333.0	3158.6
22.7	1185.4	1936.9	2485.8	1219.8	2486.2	3310.4	1362.3	2602.9	3491.5

Model-predicted von Mises stress, cumulative stress, and strain (10th, 50th, and 90th percentile) on the posterior wall of the mid-diaphysis of the left leg, when subjects walked without a load (0.0 kg), or with an additional load of 11.3 kg (25 lb) or 22.7 kg (50 lb), for the short woman, medium woman, and tall woman.

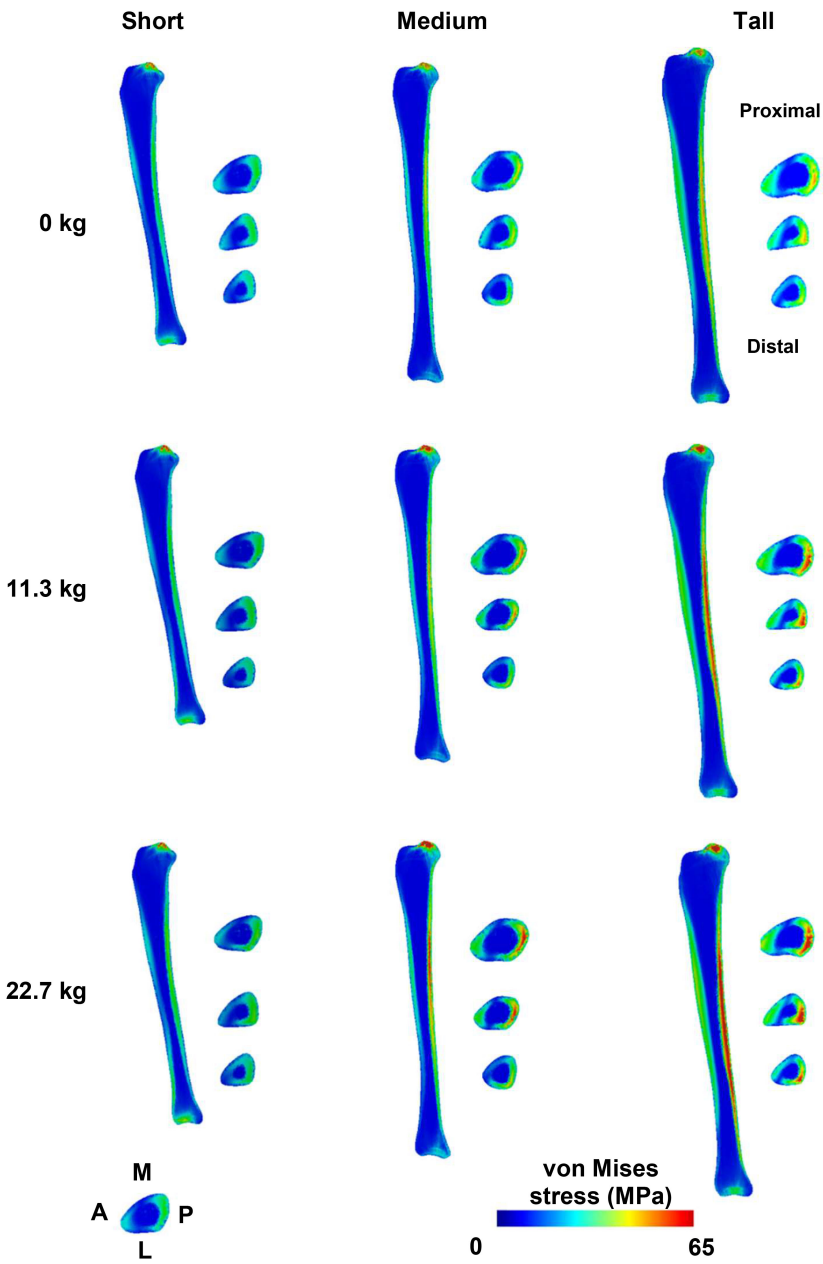

Fig. 5. Peak tibial stress distribution in a sagittal plane and three transverse (proximal-third, middle-third, and distal-third) cross-sections of the left leg of the short woman, medium woman, and tall woman walking without (top) and with an additional load of 11.3 kg (25 lb; center) or 22.7 kg (50 lb; bottom). We divided the cross section of the left tibia into four sectors: Anterior (A), Posterior (P), Medial (M), and Lateral (L). The three cross-sections correspond to the proximal third, middle-third, and distal-third sections of the tibia.

forces and bone stresses increases the risk of stress fracture, our results suggest that, the short woman has a lower risk of stress fracture compared to the medium and tall women. Although we cannot deduce the influence of height alone on the risk of stress fracture in these subjects, these results highlight the importance of subject-specific modeling of the tibia in M/FE models when subjects walk at their preferred stride length.

One limitation concerning this study is that each anthropometric group included only one subject, which precludes us from concluding that the results for each subject are representative of a specific anthropometric group. Second, we only assessed acute effects of load carriage on bone loading. We believe that it is necessary to include the biological responses to bone loading in a model before attempting to predict the occurrence of stress fracture. Third, we acquired motion-capture data when the subjects walked at their preferred stride length. However, it should be noted that certain military activities, such as marching, require locomotion with a fixed cadence, which can lead to modification of the preferred stride length in shorter and taller subjects. Fourth, although we individualized the tibial geometry and material properties, and adjusted the muscle strength based on the height, weight, and fat percentage of the individual, we

did not customize muscle strength or consider muscular fatigue. Incorporating subject- and task-specific muscle strengths into musculoskeletal models adds an important dimension of personalization, especially when considering cases such as strenuous military training, given that fatigue increases bone strain by 26% after a 2-km run and by 29% after a 30-km desert march [33]. Individualized muscular properties based on CT images and dynamic isokinetic torque measurements [33], which may improve the accuracy of injury risk estimates, should be considered in future analyses.

V. Conclusion

Here, we quantified how joint kinetics and tibial stress change owing to the individual characteristics of tibial morphology (i.e., shape and size) in three women. For each woman, we quantified the joint kinetics and tibial mechanics during walking using an individualized M/FE model. This approach characterizes the integrative effects of subject-specific characteristics known to influence the mechanical load on the tibia, including body size, tibial morphology, BMD distribution, and motion characteristics. We believe that the results from this study, along with the methodology to individualize M/FE analysis, represent a way forward to predicting the biomechanical effects of a training regimen on individuals. Such findings may provide a firm theoretical foundation for optimizing military training.

Acknowledgment

The authors would like to thank Dr. Tatsuya Oyama for editorial assistance. The authors declare no competing interests. The opinions and assertions contained herein are the private views of the authors and are not to be construed as official or as reflecting the views of the United States (U.S.) Army, the U.S. Department of Defense, or The Henry M. Jackson Foundation for the Advancement of Military Medicine, Inc. This paper has been approved for public release with unlimited distribution.

References

[1] B. H. Jones and B. C. Hansen, "An armed forces epidemiological board evaluation of injuries in the military," *Amer. J. Prev. Med.*, vol. 18, pp. 14–25, Apr. 2000.
[2] K. Bennell *et al.*, "Risk factors for stress fractures," *Sports Med.*, vol. 28, no. 2, pp. 91–122, Aug. 1999.
[3] T. J. Brudvig *et al.*, "Stress fractures in 295 trainees: A one-year study of incidence as related to age, sex, and race," *Mil. Med.*, vol. 148, no. 8, pp. 666–667, Aug. 1983.
[4] K. L. Popp *et al.*, "Bone mass, microarchitecture and strength are influenced by race/ethnicity in young adult men and women," *Bone*, vol. 103, pp. 200–208, Oct. 2017.
[5] C. Xu *et al.*, "An integrated musculoskeletal-finite-element model to evaluate effects of load carriage on the tibia during walking," *J. Biomech. Eng.*, vol. 138, no. 10, pp. 101001–101011, Oct. 2016.
[6] C. Xu *et al.*, "A cross-sectional study of the effects of load carriage on running characteristics and tibial mechanical stress: Implications for stress-fracture injuries in women," *BMC Musculoskeletal Disorders*, vol. 18, no. 1, pp. 125–136, Mar. 2017.
[7] R. Al Nazer *et al.*, "Direct in vivo strain measurements in human bone-a systematic literature review," *J. Biomech.*, vol. 45, no. 1, pp. 27–40, Jan. 2012.
[8] D. B. Burr, "Why bones bend but don't break," *J. Musculoskeletal Neuronal Interact.*, vol. 11, no. 4, pp. 270–285, Dec. 2011.
[9] K. L. Bennell *et al.*, "Models for the pathogenesis of stress fractures in athletes," *Brit. J. Sports Med.*, vol. 30, no. 3, pp. 200–204, Sep. 1996.
[10] H. M. Frost, "Bone "mass" and the "mechanostat": A proposal," *Anatomical Rec.*, vol. 219, no. 1, pp. 1–9, Sep. 1987.
[11] T. Miller *et al.*, "The classification systems of stress fractures: A systematic review," *Phys. Sportsmed.*, vol. 39, no. 1, pp. 93–100, Feb. 2011.
[12] S. J. Warden *et al.*, "Stress fractures: Pathophysiology, epidemiology, and risk factors," *Current Osteoporosis Rep.*, vol. 4, no. 3, pp. 103–109, Sep. 2006.
[13] J. Knapik *et al.*, "Stress fracture risk factors in basic combat training," *Int. J. Sports Med.*, vol. 33, no. 11, pp. 940–946, Nov. 2012.
[14] K. L. Bennell *et al.*, "Risk factors for stress fractures in track and field athletes. A twelve-month prospective study," *Amer. J. Sports Med.*, vol. 24, no. 6, pp. 810–818, Nov.–Dec., 1996.
[15] C. Milgrom *et al.*, "Stress fractures in military recruits. A prospective study showing an unusually high incidence," *J. Bone Joint Surg. Brit.*, vol. 67, no. 5, pp. 732–735, Nov., 1985.
[16] R. A. Shaffer *et al.*, "Predictors of stress fracture susceptibility in young female recruits," *Amer. J. Sports Med.*, vol. 34, no. 1, pp. 108–115, Jan. 2006.
[17] C. C. Gordon *et al.*, "2012 anthropometric survey of U.S. Army Personnel: Methods and summary statistics," U.S. Army Natick Soldier Research, Tech. Rep. NATICK/TR-15/007, 2014.
[18] K. Horsman, "The Twente lower extremity model. Consistent dynamic simulation of the human locomotor apparatus," Ph.D. thesis, Biomed. Eng. Group, Faculty Eng. Technol., Univ. Twente, Enschede, The Netherlands, 2007.
[19] V. Carbone *et al.*, "TLEM 2.0—A comprehensive musculoskeletal geometry dataset for subject-specific modeling of lower extremity," *J. Biomech.*, vol. 48, no. 5, pp. 734–741, Mar. 2015.
[20] M. A. Marra *et al.*, "A subject-specific musculoskeletal modeling framework to predict in vivo mechanics of total knee arthroplasty," *J. Biomech. Eng.*, vol. 137, no. 2, pp. 020904-1–020904-11, Feb. 2015.
[21] J. W. Fernandez *et al.*, "Anatomically based geometric modelling of the musculo-skeletal system and other organs," *Biomech. Model Mechanobiol.*, vol. 2, no. 3, pp. 139–155, Mar. 2004.
[22] M. S. Andersen *et al.*, "A computationally efficient optimisation-based method for parameter identification of kinematically determinate and over-determinate biomechanical systems," *Comput. Methods Biomech. Biomed. Eng.*, vol. 13, no. 2, pp. 171–183, Aug. 2010.
[23] M. Sangeux and J. Polak, "A simple method to choose the most representative stride and detect outliers," *Gait Posture*, vol. 41, no. 2, pp. 726–730, Feb. 2015.
[24] M. Damsgaard *et al.*, "Analysis of musculoskeletal systems in the AnyBody Modeling System," *Simul. Model Pract. Theory*, vol. 14, pp. 1100–1111, Nov. 2006.
[25] W. B. Edwards *et al.*, "Torsional stiffness and strength of the proximal tibia are better predicted by finite element models than DXA or QCT," *J. Biomech.*, vol. 46, no. 10, pp. 1655–1662, Jun. 2013.
[26] B. Helgason *et al.*, "Mathematical relationships between bone density and mechanical properties: A literature review," *Clin. Biomech.*, vol. 23, no. 2, pp. 135–146, Feb. 2008.
[27] F. Taddei *et al.*, "The material mapping strategy influences the accuracy of CT-based finite element models of bones: An evaluation against experimental measurements," *Med. Eng. Phys.*, vol. 29, no. 9, pp. 973–979, Nov. 2007.
[28] C. Sandino *et al.*, "The poro-viscoelastic properties of trabecular bone: A micro computed tomography-based finite element study," *J. Mech. Behav. Biomed. Mater.*, vol. 44, pp. 1–9, Apr. 2015.
[29] V. Carbone *et al.*, "Sensitivity of subject-specific models to errors in musculo-skeletal geometry," *J. Biomech.*, vol. 45, no. 14, pp. 2476–2480, Sep. 2012.
[30] C. Zannoni *et al.*, "Material properties assignment to finite element models of bone structures: A new method," *Med. Eng. Phys.*, vol. 20, no. 10, pp. 735–740, Dec. 1998.
[31] A. Meunier, "Mechanical aspects of bone remodeling," in *Computational Fluid and Solid Mechanics 2003*, K. J. Bathe, Ed. Oxford, U.K.: Elsevier Science, 2003, pp. 1771–1774.
[32] R. H. Miller *et al.*, "Why don't most runners get knee osteoarthritis? A case for per-unit-distance loads," *Med. Sci. Sports Exercise*, vol. 46, no. 3, pp. 572–579, Mar. 2014.
[33] C. Milgrom *et al.*, "The effect of muscle fatigue on in vivo tibial strains," *J. Biomech.*, vol. 40, no. 4, pp. 845–850, 2007.